Available online at www.sciencedirect.com
ScienceDirect
Journal of Hazardous Materials 152 (2008) 721–729
Journal of Hazardous Materials
www.elsevier.com/locate/jhazmat

Removal and recovery of gas-phase element mercury by metal oxide-loaded activated carbon

Zhijian Mei [a], Zhemin Shen [a,*], Qingjie Zhao [b], Wenhua Wang [a], Yejian Zhang [a]

[a] *School of Environmental Science and Engineering, Shanghai Jiao Tong University, 800 Dong Chuan Road, Shanghai 200240, PR China*
[b] *Shanghai Academy of Environmental Science, 508 Qin-Zhou Road, Shanghai 200233, PR China*

Received 9 January 2007; received in revised form 14 July 2007; accepted 16 July 2007
Available online 19 July 2007

Abstract

The reusability of Co_3O_4 (AC-Co), MnO_2 (AC-Mn) and $CuCoO_4$ (AC-CC) loaded activated carbon (AC) and their element mercury removal efficiency had been studied using a laboratory-scale fixed-bed reactor under simulated flue gas conditions. Tests showed that spent AC-Co could be regenerated through heating at 673 K under N_2 atmosphere and the enrichment regenerated Hg^0 could be collected to eliminate the secondary pollution. Regenerated AC-Mn and AC-CC's Hg^0 removal efficiency decreased greatly due to AC's decomposition and MnO_2's crystal structure variation. Compared with AC and metal oxides, metal oxide-loaded AC had higher Hg^0 capture ability and capacity due to AC huge surface areas and lots of function groups. TGA analysis results showed that AC-Co and AC-Mn's HgO adsorptive capacity at 523 K reached 19.8 mg g^{-1} and 5.21 mg g^{-1}, respectively. High loading values and adsorption temperatures were beneficial to AC-Co's Hg^0 removal efficiency. However, $CuCoO_4$ and MnO_2's AC decomposition ability had negative effect on AC-CC and AC-Mn's performance, respectively, especially at high adsorption temperatures and loading values. SO_2 tests showed that AC-CC had higher anti SO_2-poisoning ability than AC-Co and AC-Mn.

Keywords: Mercury; Activated carbon; Gas-phase; Metal oxide; Regeneration

1. Introduction

The environment impact of mercury released during coal combustion was significant. Of all trace metals emitted during fossil fuel combustion and waste incineration, Hg was considered as the most problematic pollutant based on many documented adverse health effects associated with Hg exposure and the inability of current pollution control technologies and strategies, designed primarily for particulated matter (PM), NO_x, and SO_2, to effectively control volatile Hg species, especially Hg^0 [1–8].

The approaches being considered for the control of mercury emission from the flue gas included sorbent injection (SI), especially activated carbon injection (ACI), and oxidation of the element mercury so as to take advantage of current control technologies [8–10]. Virgin activated carbon (AC) showed less Hg^0 capture ability, especially at high temperatures [11,12]. For this reason, chemically treated AC, such as sulfur (S), chlorine (Cl) and iodine (I) impregnated AC [13–15], were applied for the mercury emission control. However, some problems still existed: (1) AC had poor capacity for element mercury; (2) good performance was only obtained over a limited temperature range (typically below 423 K) even for sulfur impregnated AC [16]; (3) spent sorbents could not be regenerated due to $HgCl_2$, HgS and/or $HgBr_2$'s high decomposition temperature and might cause the secondary pollutions [17].

Changing element mercury into oxidized species was focused on the development of novel materials that could be used as an alternative to commercially available sorbents and oxidizing agents in order to enhance performance and reduce operating costs for the mercury control systems used at coal-fired power plants. Many metal oxides had been used to capture mercury such as CuO, Cu_2O, V_2O_5, Cr_2O_3, MnO_2, MoO_3, Fe_2O_3, TiO_2, etc. [18–21]. Granite [18] suggested that lattice oxygen of metal oxides could also serve as the oxidant of mercury. The surface area, activity of the sorbent as an oxidation catalyst, stability of lower oxides, oxygen partial pressure, and tendency to form the binary oxide could impact oxides capacity for mercury. Because

* Corresponding author. Tel.: +86 21 27977572; fax: +86 21 54742863.
E-mail address: pnyql520@hotmail.com (Z. Shen).

0304-3894/$ – see front matter © 2007 Elsevier B.V. All rights reserved.
doi:10.1016/j.jhazmat.2007.07.038

of the low mercury concentration level in the flue gas, the Hg^0 oxidation rate relied on the mass transfer driven by the concentration gradient of mercury. One method to improve oxidation rate was increasing the contact surface between metal oxides and Hg^0.

Although many works had been done to apply metal oxides to mercury emission control, how to dispose spent metal oxides to eliminate the secondary pollution was still a problem. A new method, as described in this paper, was introduced to improve AC's Hg^0 removal efficiency and eliminate potential secondary pollution. Firstly, metal oxide was loaded on AC to control gas-phase Hg^0 emission. On the one hand, metal oxide was highly dispersed by AC's huge surface. On the other hand, good performance of AC could be extended to higher temperature due to metal oxide's Hg^0 catalytic oxidation ability [22]. Secondly, spent metal oxide was regenerated through heating at 673–773 K, which made this technology advance from economic consideration. Finally, the enrichment regenerated Hg^0 could be collected using cold trap or react with other chemical reagent, such as S, to eliminate the secondary pollution [23].

In this paper, MnO_2, which had been carefully studied, was selected as an object to testify above method. However, MnO_2 had bad performance when SO_2 existed in simulated flue gas. To solve this problem, novel metal oxides Co_3O_4 and $CuCoO_4$ were also selected as research object. The performances were evaluated through varying the loading values of metal nitrate and the adsorption temperatures using a laboratory-scale adsorption fixed-bed reactor. The breakthrough time (defined as $C_0/C_i = 95\%$) of different metal oxide-loaded AC, the effect of SO_2 and the regeneration of spent sorbents through thermal decomposition under N_2 atmosphere were studied.

2. Materials and methods

2.1. Sample preparation

Lignite coal-based AC which purchased from Shanghai Reagent Corporation of China was ground and sieved to 100–120 mesh size, with a geometric mean particle diameter of around 0.2 mm. After sieving, the carbon was washed with de-ionized (DI) water, and then dried in an electric oven at 383 K for 24 h. The resulting material was stored in a desiccator prior to adsorption experiments.

AC-Mn and AC-Co were prepared by the thermal decomposition of Mn-nitrate and Co-nitrate loaded AC, respectively. At first, Mn-nitrate or Co-nitrate was dissolved in water to form the corresponding solution. In order to identify the effect of metal oxide concentrations on gas-phase Hg^0 adsorption capacity and physiochemical properties, AC was impregnated by the solution in proportion corresponding to different metal nitrate loading values (ρ) (0.5 wt.%, 1 wt.%, 5 wt.%, 10 wt.%, 15 wt.%, 20 wt.%, 25 wt.% and 30 wt.%). In order to facilitate the impregnation process, the solution was heated at 343 K with constant stirring for 2 h. After impregnation, the AC was dried in an electric oven at 383 K for 24 h and calcined at 573 K (for AC-Mn) or 673 K (for AC-Co) under N_2 atmosphere.

$CuCoO_4$ loaded AC (AC-CC) was prepared by the thermal decomposition of Cu-nitrate/Co-nitrate mixture loaded AC. Both nitrates were mixed in the Cu/Co atomic ratio of 1. The mixture was dissolved in water to form the mixture solution. AC was impregnated by the mixture solution in proportion corresponding to different Cu-nitrate/Co-nitrate mixture loading values and heated to 503 K, the temperature at which nitrogen oxides were evolved. The heterogeneous mass obtained was ground in a mortar and heated for 3 h at 673 K under N_2 atmosphere.

The preparations of blank sorbents MnO_2 (AAO-Mn), $CuCoO_4$ (AAO-CC) and Co_3O_4 (AAO-Co) loaded on active aluminum oxide (AAO) were similar to the corresponding AC-Mn, AC-CC and AC-Co, except that AC was replaced by AAO. All chemicals used above were analytical grade.

2.2. Analytic methods

The X-ray diffractogram (XRD) patterns obtained on a Bruker D8 Advance with X-ray diffractometer using Cu Kα radiation as X-ray source were used to determine the crystallite identity. The accelerating voltage and the applied current were 40 kV and 40 mA, respectively. The Brunauer–Emmett–Teller (BET) specific surface area (S_{BET}) and pore size distribution were determined using a Micromeritics ASAP 2010 nitrogen adsorption apparatus. All the sorbents were degassed at 453 K prior to BET measurements. The thermogravimetric analysis (TGA) was performed with TGA 2050 thermal analyzer. The accuracies of weighing and temperature measurements were within 0.1 μg and 0.25 °C, respectively. The thermometer was calibrated at the triple point of water (0.01 °C) and at the freezing point of indium (156.5985 °C). The spent sorbents were placed in an open platinum pan and the experiments conducted in N_2 at a flow rate of 50 mL min^{-1}. Different from the work of Lin which kept the temperature at certain degree [12], nominal heating rate of 20 K min^{-1} was employed to increase the desorption temperature from 293 K to 1073 K and continuous records of temperature and sorbent weight were taken. The vapor-phase Hg^0 concentrations were analyzed continuously using a SG-921 cold vapor atomic absorption spectroscopy (CVAAS). The total mercury concentration of spent sorbents was determined using AMA254 advanced mercury analyzer. AMA254 is a single purpose atomic absorption spectrophotometer for mercury determination. It is designated for the direct mercury determination in solid and liquid sorbents without a need of sorbent chemical pre-treatment (mineralization, etc.)

2.3. Catalytic test

The assembly used for adsorption test consisted of an element mercury permeation tube, a packed-bed reactor, an on-line cold vapor atomic absorption spectroscopy, and a data acquisition system. The reactor scheme was shown in Fig. 1. A flow of simulated flue gas passed over the permeation tube and yielded a stable concentration of mercury. The reactor (adsorber) was a quartz tube (760 mm in length with an outer

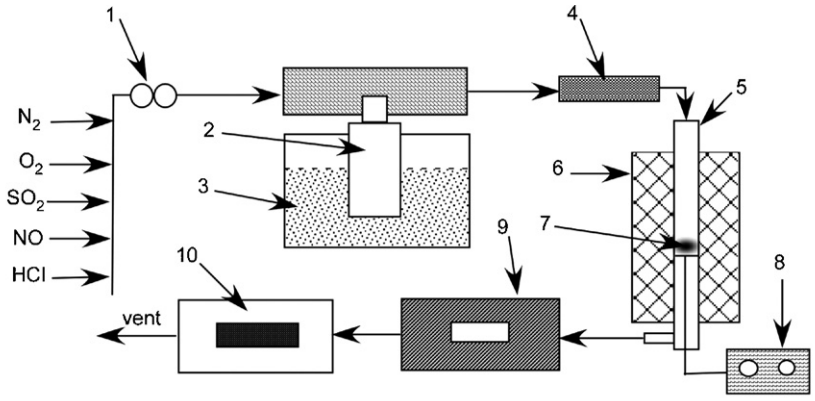

1. Mass Flow Control; 2. Hg^0 Permeation Tube; 3. Oil Heating Bath; 4. Heating Tape; 5. Tubular Reactor; 6. Furnace; 7. Catalyst; 8. Temperature Monitor; 9. CVAAS; 10. Activated Carbon Trap.

Fig. 1. Schematic of the experimental setup. CVAAS – SG-921 cold vapor atomic absorption spectrophotometry detects the gas-phase Hg^0 concentration on line. Mass flow meter – control the quantity of gas flow. Hg permeation tube – control Hg^0 emission rate. Tubular reactor – the main reaction place where sorbents are placed and adsorption temperature is under control. Activated carbon trap – capture the mercury in the effluent to eliminate pollution.

diameter of 5.08 mm and inner diameter of 4.2 mm) held in a vertical position. Quartz had good chemical resistance and inertness toward element mercury. The reactor was surrounded by a large clam-shell furnace. A temperature control device was employed to keep the adsorbent bed at desired temperature. Simulated gas passed through permeation tube holder and then directly went to the CVAAS to determine the baseline of Hg^0 concentration. Once thermal stability reached, simulated gas was diverted to pass through adsorbent bed for the test.

Some kinetic parameters for Hg^0 adsorption test were obtained under condition 1 with inlet gas flow rate of $6\,L\,h^{-1}$ and empty bed contact time (EBCT) of 0.046 s. The compositions of the inlet gas were listed in Table 1. The catalyst mass was 0.015 g and the length of catalyst bed was between 0.5 mm and 0.7 mm. The studies were carried out at different adsorption temperatures (373–523 K) and the Hg^0 concentration of influent or effluent was determined using SG-921. For SO_2 test, the experiment was carried out under condition 2 whose gas composition was similar to coal-fire power plant flue gas (Table 1). Unless specified, the run time of each test was 2 h. For spent sorbents regeneration, the high-purity nitrogen (>99.999%) was introduced as protective gas.

Table 1
The gas composition of condition 1 and condition 2 for test

Gas	Concentration in the condition 1	Concentration in the condition 2
O_2	5.0 vol.%	5.0 vol.%
N_2	Balance	Balance
SO_2	0	0.31 vol.%
NO	0	0.23 vol.%
CO	0	0.158 vol.%
HCl	0	0.0035 vol.%
Hg^0	1.26 ppm	0.035 ppm

3. Results and discussion

3.1. Catalyst characterization

Pore characteristics are one of the most important factors contributed to removal efficiency as pores allow rapid diffusion of various gaseous reactants and products during Hg^0 oxidation reaction and enhance the oxidation rate. Pore-size distribution of various types of ameliorated AC and AAO was calculated using Barrett–Joyner–Halenda (BJH) method. Their pore characteristics were shown in Table 2. It could be seen that pore volume and pore size became smaller with the increase of metal oxide's loading values. Virgin AC had the highest S_{BET} value of $849.8\,m^2\,g^{-1}$, the highest pore volume of $0.47\,mL\,g^{-1}$ and the largest pore size of 2.21 nm. When loaded with 5 wt.% Co-nitrate, $S_{BET,}$ pore volume and pore size decreased to $805.4\,m^2\,g^{-1}$, $0.42\,mL\,g^{-1}$ and 2.11 nm, respectively. When loaded with 20 wt.% Co-nitrate, S_{BET} and pore volume decreased to $744.5\,m^2\,g^{-1}$ and $0.38\,mL\,g^{-1}$, respectively. At the same time, pore size kept around 2.14 nm. Therefore, when Co-nitrate loading value increased from 5 wt.% to 20 wt.%, metal oxide conglomeration mainly located on the

Table 2
Effect of metal oxides on the BET surface area and pore parameters of activated carbon

Sample	Surface area ($m^2\,g^{-1}$)	Pore volume ($mL\,g^{-1}$)	Pore size (nm)
AC	849.8	0.47	2.21
AC-CC	746.7	0.39	2.04
AC-Co-20	744.5	0.38	2.14
AC-Co-5	805.4	0.42	2.11
AC-Mn-20	746.1	0.40	2.13
AC-Mn-5	805.1	0.43	2.09
AAO-Co	74.2	0.183	14.6
AAO-Mn	73.2	0.179	14.2

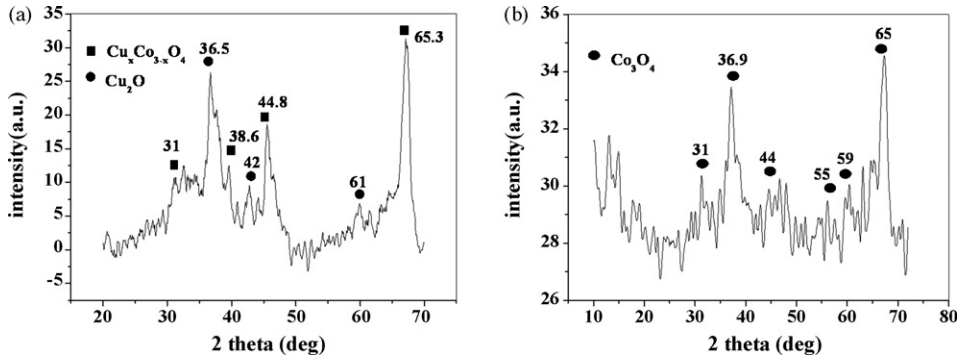

Fig. 2. The XRD patterns of (a) AAO-CC, (b) AAO-Co. (■) $Cu_xCo_{3-x}O_4$ – the XRD peaks of $Cu_xCo_{3-x}O_4$. (●) Cu_2O – the XRD peaks of Cu_2O. (●) Co_3O_4 – the XRD peaks of Co_3O_4.

surface of AC, little in the pores. The situation of AC loaded with MnO_2 or $CuCoO_4$ was similar to AC-Co.

X-ray diffractograms (XRD) (Fig. 2) of AAO-CC and AAO-Co were analyzed using crystallographic search-match and the results were shown in Table 3. It could be seen that, although different $Cu_xCo_{3-x}O_4$ ($x<1$) and Cu_xO existed in AAO-CC, their patterns were all cubic spinel. Cubic spinels with copper atoms, $Cu_{0.15}Co_{2.85}O_4$ (Cube), $Cu_{0.75}Co_{2.25}O_4$ (Cube) $Cu_{0.95}Co_{2.05}O_4$ (Cube), $CuCo_2O_4$ (Cube) were identified when adulterated with Cu. It was implied that many introduced copper atoms in the spinel phase may increase Hg^0 oxidation ability. For AAO-Co, there existed mainly Co_3O_4.

3.2. Effect of loading value

Relationships between Hg^0 removal efficiency (η) and metal nitrate loading value (ρ) of AC-Co, AC-CC and AC-Mn were investigated. The results were shown in Fig. 3, wherein ρ is defined as follows:

$$\rho = \frac{W_{\text{nitrate}}}{W_{\text{AC}}} \times 100\% \quad (1)$$

wherein W_{AC} is the quantity of AC (g), W_{nitrate} is the quantity of metal nitrate load on AC (g).

η is defined as follows:

$$\eta = \frac{\text{Hg}_{\text{inlet}} - \text{Hg}_{\text{outlet}}}{\text{Hg}_{\text{inlet}}} \times 100\% \quad (2)$$

wherein Hg_{inlet} is the concentration of inlet Hg^0 (g m^{-3}), Hg_{outlet} is the concentration of outlet Hg^0 (g m^{-3}).

When loaded with metal oxide, sorbent's Hg^0 removal efficiency increased (Fig. 4). Virgin AC had the least Hg^0 removal efficiency at 523 K among the tested sorbents. When loading value was below 5 wt.%, AC-Mn showed higher Hg^0

Table 3
The XRD analysis results of AAO-CC and AAO-Co

Sample	The possible phase (strong → weak)
AAO-CC	Cu_2O (cube) → $Cu_{0.15}Co_{2.84}O_4$ (cube) → $Cu_{0.75}Co_{2.25}O_4$ (cube) → $Cu_{0.95}Co_{2.05}O_4$ (cube) → $CuCo_2O_4$ (cube)
AAO-Co	Co_3O_4

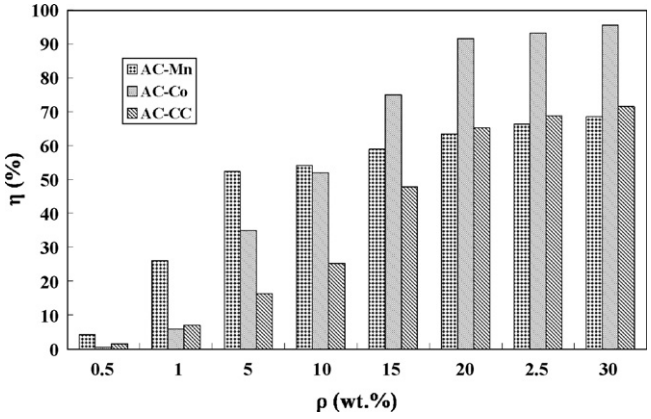

Fig. 3. Effect of metal nitrate loading value ρ on AC's mercury removal efficiency under condition 1 at 523 K. AC-M – effect of Mn-nitrate loading value on AC's mercury removal efficiency under condition 1 at 523 K. AC-Co – effect of Co-nitrate loading value on AC's mercury removal efficiency under condition 1 at 523 K. AC-CC – effect of Co-nitrate and Cu-nitrate loading value on AC's mercury removal efficiency under condition 1 at 523 K.

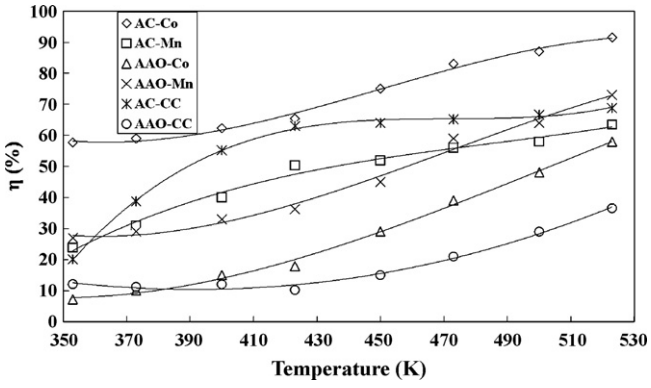

Fig. 4. Hg^0 removal efficiency vs. adsorption temperature of different 20 wt.% metal nitrates loaded AC under condition 1. AC-M – Hg^0 removal efficiency vs. adsorption temperature of 20 wt.% Mn-nitrate loaded AC under condition 1. AC-Co – Hg^0 removal efficiency vs. adsorption temperature of 20 wt.% Co-nitrate loaded AC under condition 1. AC-CC – Hg^0 removal efficiency vs. adsorption temperature of 20 wt.% Co-nitrate and Cu-nitrate loaded AC under condition 1. AAO-M – Hg^0 removal efficiency vs. adsorption temperature of 20 wt.% Mn-nitrate loaded AAO under condition 1. AAO-Co – Hg^0 removal efficiency vs. adsorption temperature of 20 wt.% Co-nitrate loaded AAO under condition 1. AAO-CC – Hg^0 removal efficiency vs. adsorption temperature of 20 wt.% Co-nitrate and Cu-nitrate loaded AAO under condition 1.

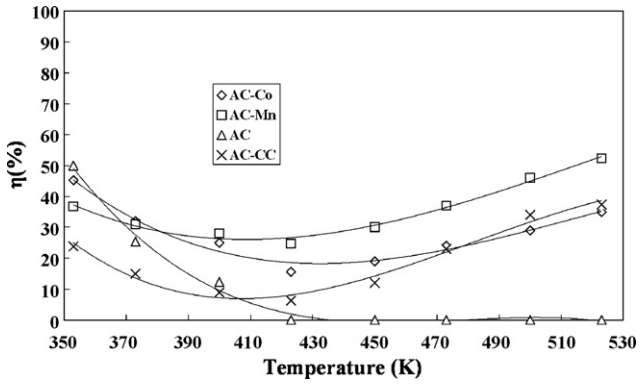

Fig. 5. Hg^0 removal efficiency vs. adsorption temperature of different 5 wt.% metal nitrates loaded AC under condition 1. AC-M – Hg^0 removal efficiency vs. adsorption temperature of 5 wt.% Mn-nitrate loaded AC under condition 1. AC-Co – Hg^0 removal efficiency vs. adsorption temperature of 5 wt.% Co-nitrate loaded AC under condition 1. AC-CC – Hg^0 removal efficiency vs. adsorption temperature of 5 wt.% Co-nitrate and Cu-nitrate loaded AC under condition 1. AC – AC's Hg^0 removal efficiency at different adsorption temperatures under condition 1.

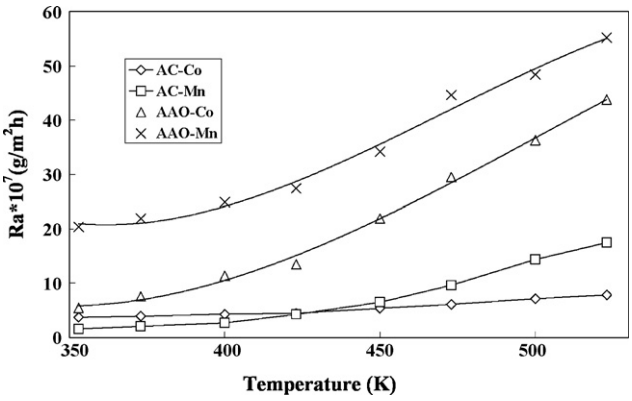

Fig. 6. Average oxidation rate Ra vs. adsorption temperature T of different 20 wt.% metal nitrates loaded AC under condition 1. AC-Co – average oxidation rate Ra vs. adsorption temperature T of 20 wt.% Co-nitrate loaded AC under condition 1. AC-Mn – average oxidation rate Ra vs. adsorption temperature T of 20 wt.% Mn-nitrate loaded AC under condition 1. AAO-Co – average oxidation rate Ra vs. adsorption temperature T of 20 wt.% Co-nitrate loaded AAO under condition 1. AAO-Mn – average oxidation rate Ra vs. adsorption temperature T of 20 wt.% Mn-nitrate loaded AAO under condition 1.

removal efficiency than AC-Co and AC-CC. When loading value increased above 5 wt.%, AC-Co's Hg^0 removal efficiency increased obviously higher than AC-Mn's. This inconsistency was attributed to MnO_2's AC decomposition which was discussed later and high loading value was beneficial to this effect. Because $CuCoO_4$ could also catalytic decompose AC, AC-CC's performance was similar to AC-Mn. In later study, 20 wt.% was selected as default metal nitrate loading value due to the high Hg^0 removal efficiency.

3.3. Temperature effect

The performances of different metal oxide-loaded AC under different adsorption temperatures (353–523 K) were analyzed to study the temperature effect. The results were shown in Fig. 4 and Fig. 5. When loading value was 5 wt.%, AC-Mn, AC-CC and AC-Co had the minimum Hg^0 removal efficiency at 423 K due to the low mercury oxidation rate of AC and metal oxide. When loading value reached 20 wt.%, the minimum point disappeared due to the improvement of Hg^0 oxidation rate which was catalyzed by metal oxide. Increasing adsorption temperature from 423 K to 523 K, AC-Mn and AC-CC's Hg^0 removal efficiency kept basically stable and AC-Co's Hg^0 removal efficiency increased from 65.4% to 91.5%.

By contrast, the performances of AAO carrier sorbents, including AAO-Co, AAO-CC and AAO-Mn, were investigated under the same adsorption conditions. For AAO carrier sorbents, Hg^0 removal efficiency greatly improved with the increase of adsorption temperature, as shown in Fig. 4. AC carrier sorbents had higher Hg^0 removal efficiency than AAO carrier sorbents due to their huge specific surface areas. However, when the adsorption temperature reached 523 K, AAO-Mn's Hg^0 removal efficiency exceeded AC-Mn for the first time. This inconsistent variation trend could be explained as follow: firstly, AC had negative effect on MnO_2's Hg^0 oxidation ability which would greatly decrease AC-Mn Hg^0 removal efficiency. This could be inferred from Fig. 4 where AAO-Mn showed the highest Hg^0 removal efficiency among AAO carrier sorbents and AC-Co showed the maximum activity among AC carrier sorbents. Secondly, AC's porous structure and function groups could be destroyed due to MnO_2 catalytic decomposition at high temperatures (Table 4) and the decomposition products would affect the activity of MnO_2 through covering and/or reacting with the activated centers.

Taking into account of the specific surface areas of different sorbents, the average oxidation rate Ra versus adsorption temperature T was shown in Fig. 6. Wherein Ra is defined as

Table 4
The weight and surface variation of different samples after 2 h adsorption test at different temperatures

Sample		353 K	373 K	400 K	423 K	450 K	473 K	500 K	523 K
AC-CC	Weight (%)	100	98.6	97.3	96	80.7	76	74.7	68.7
	S_{BET} ($m^2\ g^{-1}$)	746	743.2	742.5	736	581.2	527.2	455.1	346.7
AC-Mn	Weight (%)	100	98.6	98	91.3	77.8	67.8	64.4	61.7
	S_{BET} ($m^2\ g^{-1}$)	768	765.4	764.3	658.9	519.6	434.4	316.3	297.4
AC-Co	Weight (%)	100	98	95.4	96	93.4	92	88.7	87.4
	S_{BET} ($m^2\ g^{-1}$)	772	769	763.3	763.5	747.3	734	687.3	668.3

Table 5
Comparison of Hg capture ability (θ) with Hg removal efficiency (η) of different materials under condition 1 at 523 K and the mass balance of Hg during the absorption and desorption tests

Sample	η (%)	θ (%)	ζ[a] (%)	Out gas (%)		Sorbents (%)			Out/in (%)	Breakthrough time (h)
				Hg^0	Hg^{2+}	Hg^0	HgO	Hg^{2+}		
AC	N/A	N/A	N/A	N/A	N/A	N/A	N/A	N/A	N/A	<1
AC-Co	91.5	90.5	1	8.5	0.8	1.2	82	3.5	96	119
AC-Mn	63.5	61.8	2.8	36.5	1.6	1.4	50.7	2.8	93	40
AC-CC	65.2	63.4	2.76	34.8	1.5	3.5	52.8	2.4	95	24
AAO-Co	58	45.7	21.2	42	11.8	0.3	43.7	0.2	98	10
AAO-Mn	73	65.8	9.9	27	6.9	0.5	63.5	0.1	98	14
AAO-CC	36.5	30.1	17.5	63.5	6.2	1.5	25.4	0.4	97	26

[a] The oxidize mercury escape ability is defined as $(\eta - \theta)/\eta$.

formula (3):

$$\mathrm{Ra} = \frac{V \times C \times \eta}{P \times S} \quad (3)$$

wherein V is the inlet gas flow ($m^3\,h^{-1}$), C is the inlet concentration of Hg^0 ($g\,m^{-3}$), η is the Hg^0 removal efficiency, P is the sorbent charge (g) after 2 h adsorption test (Table 4) and S is the sorbent specific area ($m^2\,g^{-1}$) after 2 h adsorption test (Table 4).

Adsorption temperature had little effect on the Ra of AC-Co due to its even dispersal which made its Hg^0 oxidation rate relied on the mass transfer driven by the concentration gradient of mercury. AAO-Mn and AAO-Co's Ra increased greatly when adsorption temperature increased which indicated that AAO-Mn and AAO-Co's Ra relied on the surface reaction. For AC-Mn, when adsorption temperature below 423 K, its Ra kept basically stable. With continuous increase of adsorption temperature above 423 K, AC-Mn's Ra variation trend was similar to AAO-Mn and AAO-Co due to its specific surface area decrease.

3.4. Mercury adsorption analysis

Oxidized mercury had been found in the effluent using chloride-impregnated activated carbon as sorbent under down-flow fix-bed conditions and the total contribution of oxidized mercury species (Hg_x^0) in the effluent increased significantly with the increase in chloride content. Release of oxidized mercury forms into the effluent could be the result of either a weak carbon–chloride bond or weak chloride–mercury bond or both [13]. Therefore, it was necessary to take into account of the actual Hg captured by different sorbents and this was done by calculating the Hg capture ability (θ) of different sorbents according to formula (4):

$$\theta = \frac{q}{Q} \times 100\% \quad (4)$$

wherein q is the total quantity of Hg captured by different sorbents (g) which analyzed by AMA254, Q is the total inlet quantity of Hg^0 (g) which is estimated by

$$Q = V \times C \times t \quad (5)$$

wherein t is the adsorption time (h), V is the gas flow ($m^3\,h^{-1}$), C is influent concentration of Hg^0 ($g\,m^{-3}$).

The Hg capture ability (θ) versus Hg removal efficiency (η) was listed in Table 5. Although AAO-Mn's η and θ were greater than AC-Mn, its ζ was far less than AC-Mn. For other AC carrier sorbents, their ζ was also far less than the corresponding AAO carrier sorbents. Therefore, replacing carrier AAO with AC could greatly improve metal oxide's Hg^0 capture ability.

The times required for different sorbents to reach 95% element mercury breakthrough were listed in Table 5. AC carrier sorbent's breakthrough time was longer than corresponding AAO carrier sorbent due to its higher specific surface area. However, AC-CC's breakthrough time was shorter than AAO-CC. This inconsistent variation trend could be attributed to $CuCoO_4$'s AC decomposition ability. The AC decomposition products could affect the activity of metal oxides through covering and/or reacting with the activated centers. Compared with AC-Mn, the AC decomposition products had greater effect on AC-CC's Hg^0 oxidation ability because AC-Mn's breakthrough time was longer than AAO-Mn. This result could also infered from Fig. 4 where AC-CC's Hg^0 removal efficiency increased only 5.8% and AC-Mn's Hg^0 removal efficiency increased 13.5% when adsorption temperature increased from 423 K to 523 K. AC decomposition products had greater effect on AC-CC's activity than on AC-Mn which might be attributed to the complexity of AC-CC's activated centers.

TGA was rarely used for the adsorption of vapor-phase Hg^0. Lin et al. used TGA to determine the adsorptive capacity and adsorption isotherm of vapor-phase mercury chloride on powdered activated carbon [11,12]. In this study, we used TGA to analyze the adsorbed mercury species of spent sorbents. TGA temperature vs. sorbent weight was shown in Fig. 7 where the temperature ranges could be divided into three parts: a (<350 K), b (700–950 K) and c (950–1073 K).

The lost weight below 350 K was due to water evaporation. The lost weight between 700 K and 950 K was attributed to HgO decomposition. The reasons causing the weight lost between 950 K and 1073 K were complex, including decomposition of AC function groups which was manifested by the blank test of virgin VC. Obviously, virgin AC adsorbed lots of water due to its porous structure. The lost weight fraction of spent AC-Mn was far less than that of spent AC and AC-Co, especially below 350 K. From Fig. 7, we could inferred that AC-Co's porous structure got minor breakage and the function groups of AC had not decomposed, but AC-Mn's porous structure and function

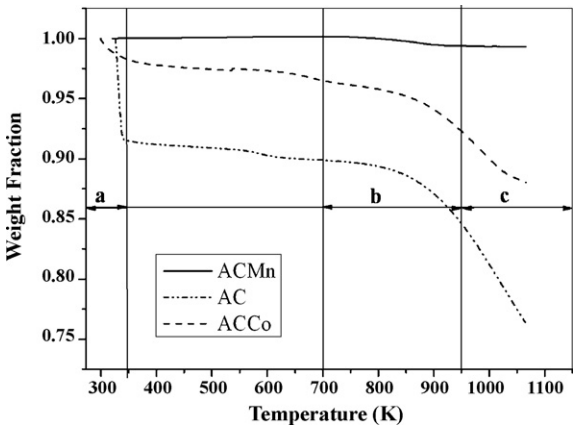

Fig. 7. TGA analysis of different spent metal oxide-loaded AC. (a) Stand for the adsorption temperature range < 350 K. (b) Stand for the adsorption temperature range 700–950 K. (c) Stand for the adsorption temperature range 950–1073 K. ACMn – the TGA curve of spent AC-Mn. AC – the TGA curve of AC. ACCo – the TGA curve of spent AC-Co.

groups were all destroyed. To clarify AC-Mn's performance, its enlarged curve was shown in Fig. 8. The lost weight fraction of spent AC-Mn between 700 K and 950 K reached 0.521 wt.% (5.21 mg g^{-1} HgO or 4.824 mg g^{-1} Hg) which was attributed to adsorbed HgO decomposition. Compared with MnO_2/Al_2O_3's 2.2 mg g^{-1} (399 K) [18] and AC's 0.23 mg g^{-1} (423 K) [11], AC-Mn's capacity had been greatly improved even at higher adsorption temperature (523 K). AC-Co had higher capacity than AC-Mn due to its higher Hg^0 capture ability and longer breakthrough time. Its maximum adsorptive capacity, in our test, reached 19.8 mg g^{-1}.

The mass balance of mercury during the adsorption tests was listed in Table 5. The quantity of inlet gas element mercury was considered as 100% and the Hg^{2+} stood for compound mercury. The mercury species on the surface of sorbents was analyzed through TGA where the enrichment regenerated Hg^0 was adsorbed by AC at ambient temperature and analyzed by AMA254. The Hg^0 concentrations at a, b and c temperature range were considered as Hg^0, HgO and Hg^{2+} adsorbed by sorbents, respectively. The mass balances varied between 93% and 98% and average 96%. AC carrier sorbents released less compound mercury than AAO carrier sorbents in the outlet gas which was consistent with their mercury capture ability results. Among AAO carrier sorbents, AAO-CC adsorbed the greatest quantity of Hg^0. The other observation was AC carrier sorbents adsorbed more element mercury than corresponding AAO carrier sorbents, especially AC-CC. Compared with AAO carrier sorbents, AC carrier sorbents adsorbed a little quantity of other compound mercury except HgO. This phenomenon might be explained as follow: firstly, for AC, there existed lots of other elements such as S, Cl which could react with mercury; secondly, the regenerated Hg^0 might be delayed to release into outlet gas due to AC's porous structure.

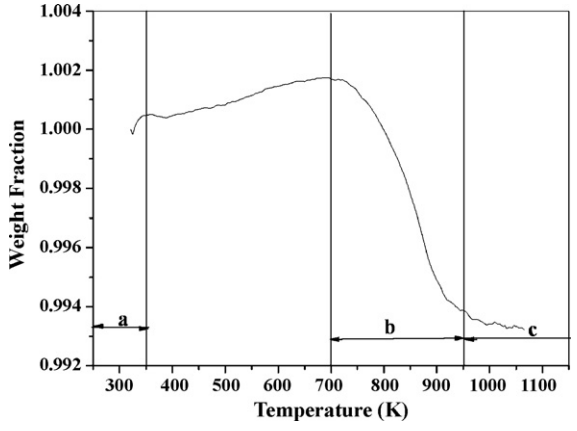

Fig. 8. TGA analysis of spent AC-Mn. (a) Stand for the adsorption temperature range < 350 K. (b) Stand for the adsorption temperature range 700–950 K. (c) Stand for the adsorption temperature range 950–1073 K.

3.5. Regeneration

For controlling mercury emissions from the flue stacks of coal-burning electric utilities, numerous advanced mercury control technologies such as sorbent injection and in situ mercury oxidation had been developed. Although these technologies could effectively remove mercury from the flue stack, they shared, along with many other technologies, the common shortcoming of intermedia pollution transfer [15].

In this part, the regenerations of spent AC-Co, AC-CC and AC-Mn under nitrogen atmosphere were discussed. The enrichment regenerated Hg^0 was captured by activated carbon at ambient temperature. The regeneration tests were conducted under condition 1 and the results were listed in Table 6.

If regeneration temperature was higher than activation temperature, sorbents' activity would be affected through crystal structure variation. After the first regeneration under nitrogen atmosphere at 723 K for 10 h, the Hg^0 removal efficiency of AC-Co decreased from 91.5% to 85.5%. After the second and third regeneration, the Hg^0 removal efficiency of AC-Co kept basically stable. The minor deactivation of AC-Co was attributed to the integrated effects of Co_3O_4 crystal structure variation and AC porous structure breakage. Compared with regenerated AC-Co, the Hg^0 removal efficiency of regenerated AC-Mn and AC-CC decreased more quickly. So AC-Co was more suitable to regeneration than AC-Mn and AC-CC.

Our previous work indicated that both Hg^0 removal efficiency and stability of AAO-CC were enhanced when regeneration times increased which might be attributed to Hg-doped $CuCoO_4$ formation during the regeneration process (data not published). We thought regenerated AC-CC's activity decrease should be attributed to AC decomposition which destroyed AC porous structure and $CuCoO_4$'s activated centers. A possible solution was using other huge surface materials which could resist high temperature such as sepiolite to replace AC.

3.6. SO_2 effect

The components in the real coal combustion flue gas such as SO_2 could react with the metal oxide on AC and made it ineffective. Therefore, the effect of SO_2 on AC-Co, AC-Mn and AC-CC's performance was very important. It was found convenient to characterize the resistance using following exper-

Table 6
The Hg^0 removal efficiency of the samples with different regeneration limes at 523 K under condition l and the influence of SO_2 on conversion efficiency over different samples under condition 2

Sample	1st Regeneration (%)		2nd Regeneration (%)		3rd Regeneration (%)		R_{SO_2}
	η	S_{BET} ($m^2\ g^{-1}$)	η	S_{BET} ($m^2\ g^{-1}$)	η	S_{BET} ($m^2\ g^{-1}$)	
AC-Co	85.5	663.2	83.4	642.5	82.2	635.4	0.12
AC-Mn	33.1	253.8	29.4	231.7	25.2	205.9	0
AC-CC	43.4	325.2	42.3	311.4	42.6	296.8	0.87

imental test. From the curve presented in Fig. 5, the temperature where the highest Hg^0 removal efficiency was attained could be determined. For every sorbent, the corresponding temperature had been adjusted. After stabilizing the conversion ($\eta^{max}_{initial}$), SO_2 was introduced into the inlet gas mixture for 120 min. At the end of this test period, the reduced conversion rate ($\eta^{reduced}_{final}$) was checked. Then, the ratio $R_{SO_2} = \eta^{reduced}_{final}/\eta^{max}_{initial}$ served as an index for measuring the resistance of sorbents towards SO_2 poisoning. The R_{SO_2} of different sorbents studied in condition 2 varied from 0 to 0.87 (Table 6).

As could be seen, AC-Co and AC-Mn lost their activity quickly when 0.31 vol.% SO_2 was introduced into the simulated flue gas. However, AC-CC possessed better resistance to SO_2 poisoning than AC-Co and AC-Mn. In previous works, it was known that, when the x of $Cu_xCo_{3-x}O_4$ ($x<1$) above 0.2, the Cu^{2+} ions were distributed over both tetrahedral and octahedral cationic sites of the spinel lattice [24]. Therefore, the poison resistant active sites could be correlated to both Co^{3+} and Cu^{2+}-octahedral cations on the surface of the spinels [25]. The results of SO_2 poisoning test indicated that AC-Co and AC-Mn could only be applied to the situation where no SO_2 existed and could not directly be applied to the real coal combustion flue gas.

4. Conclusions

In this paper, three kinds of metal oxide-loaded activated carbons were investigated to remove gas-phase element mercury. AC-Co showed the best performance under condition 1. AC-CC and AC-Mn's Hg^0 removal efficiency had been greatly affected by $CuCoO_4$ and MnO_2's AC decomposition ability. However AC-Co and AC-Mn lost their Hg^0 removal efficiency after 2 h test when SO_2 existed in the simulated gas. Therefore, AC-Co and AC-Mn could only apply to the situation where no SO_2 existed. AC-CC could be applied to actual situation due to their perfect SO_2 anti-poisoning ability. Future works would be concentrated on improving $CuCoO_4$'s Hg^0 removal efficiency and using other huge surface materials which were inexpensive and could resist high temperatures as carrier. Promising sorbent candidates would be further evaluated on a pilot-scale system.

Acknowledgment

We express our thanks to the National Nature Science Foundation of China (No. 90510009) for their support.

References

[1] G.M. Vandal, W.F. Fitzgerald, Variations in mercury deposition to Antarctica over the past 34,000 years, Nature 362 (1993) 621–623.
[2] W.K. Anger, T.J. Keefe, J. Mitchell, J.S. Reif, J.D. Tessari, L. Metzger, R. Amler, T.A. Tsongas, Two-stage evaluation of exposure to mercury and biomarkers of neurotoxicity at a hazardous waste site, J. Tox. Environ. Heal. 40 (1993) 413–422.
[3] R.P. Mason, W.F. Fitzgerald, F.M.M. Morel, The biogeochemical cycling of elemental mercury: anthropogenic influences, Geochim. Cosmochim. Acta 58 (1994) 3191–3198.
[4] J. Werther, Gaseous emissions from waste combustion, J. Hazard. Mater. (2007).
[5] V.M. Fthenakis, F.W. Lipfert, P.D. Moskowitz, L. Saroff, An assessment of mercury emissions and health risks from a coal-fired power plant, J. Hazard. Mater. 44 (1995) 267–283.
[6] Q. Wang, W. Shen, Z. Ma, Estimation of mercury emission form coal combustion in China, Environ. Sci. Technol. 34 (2000) 2711–2713.
[7] D. Van Velzen, H. Langenkamp, G. Herb, Review: mercury in waste incineration, Waste Manage. Res. 20 (2002) 556–568.
[8] P.S. Nolan, K.E. Redinger, G.T. Amrhein, G.A. Kudla, Demonstration of additive use for enhanced mercury emissions control in wet FGD systems, Fuel Proc. Technol. 85 (2004) 587–600.
[9] S. Wang, H. Wu, Environmental-benign utilisation of fly ash as low-cost adsorbents, J. Hazard. Mater. B136 (2006) 482–501.
[10] B.S. Inbaraj, N. Sulochana, Mercury adsorption on a carbon sorbent derived from fruit shell of *Terminalia catappa*, J. Hazard. Mater. B133 (2006) 283–290.
[11] H.Y. Lin, C.S. Yuan, W.C. Chen, C.H. Hung, Determination of the adsorptive capacity and adsorption isotherm of vapor-phase mercury chloride on powdered activated carbon using thermogravimetric analysis, J. Air Waste Manage. 56 (2006) 1550–1557.
[12] H.Y. Lin, C.S. Yuan, C.H. Wu, C.H. Hung, The adsorptive capacity of vapor-phase mercury chloride onto powdered activated carbon derived from waste tires, J. Air Waste Manage. 56 (2006) 1558–1566.
[13] R.D. Vidic, D.P. Siler, Vapor-phase element mercury adsorption by activated carbon impregnated with chloride and chelating agents, Carbon 39 (2001) 3–14.
[14] S.B. Ghorishi, M.K. Robert, D.S. Shannon, K.G. Brian, S.J. Wojciech, Development of a Cl-impregnated activated carbon for entrained-flow capture of element mercury, Environ. Sci. Technol. 36 (2002) 4454–4459.
[15] H. Zeng, F. Jin, J. Guo, Removal of elemental mercury from coal combustion flue gas by chloride-impregnated activated carbon, Fuel 83 (2004) 143–146.
[16] S.J. Lee, Y.C. Seo, J.S. Jurng, T.G. Lee, Removal of gas-phase elemental mercury by iodine- and chlorine-impregnated activated carbons, Atmos. Environ. 38 (2004) 4887–4893.
[17] P.T. Bolger, D.C. Szlag, An electrochemical system for removing and recovering elemental mercury from a gas stream, Environ. Sci. Technol. 36 (2002) 4430–4435.
[18] E.J. Granite, H.W. Pennline, R.A. Hargis, Novel srobents for mercury removal from flue gas, Ind. Eng. Chem. Res. 39 (2000) 1020–1029.
[19] J.W. Portzer, J.R. Albritton, C.C. Allen, R.P. Gupta, Development of novel sorbents for mercury control at elevated temperatures in coal-derived syn-

gas: results of initial screening of candidate materials, Fuel Proc. Technol. 85 (2004) 621–630.
[20] A.A. Presto, E.J. Granite, Survey of catalysts for oxidation of mercury in flue gas, Environ. Sci. Technol. 40 (2006) 5601–5609.
[21] Y. Zhao, M.D. Mann, J.H. Pavlish, B.A.F. Mibeck, G.E. Dunham, E.S. Olson, Application of gold catalyst for mercury oxidation by chlorine, Environ. Sci. Technol. 40 (2006) 1603–1608.
[22] E.S. Olson, S.J. Miller, R.K. Sharma, G.E. Dunham, S.A. Benson, Catalytic effects of carbon sorbents for mercury capture, J. Hazard. Mater. 74 (2000) 61–79.
[23] Z.M. Shen, Z.J. Mei, J.P. Chen, T. Yuan, W.H. Wang, Catalytic oxidation system for controlling mercury emission from flue gas (2005), 200510024939.2 (CN1698931).
[24] G.M. Vandal, W.F. Fitzgerald, Study of copper-cobaltite spinel formation during simultaneous decomposition of copper and cobaltous nitrates, Thermochim. Acta 67 (1983) 91–102.
[25] S. Angelov, D. Mehandjiev, B. Piperov, V. Zarkov, A. Terlecki-Baricevic, D. Jovanovic, Z. Jovanovic, Carbon monoxide oxidation on mixed spinels $Cu_xCo_{3-x}O_4$ ($0 < x < 1$) in the presence of sulphur compounds, Appl. Catal. 16 (1985) 431–437.